ChemComm

Accepted Manuscript

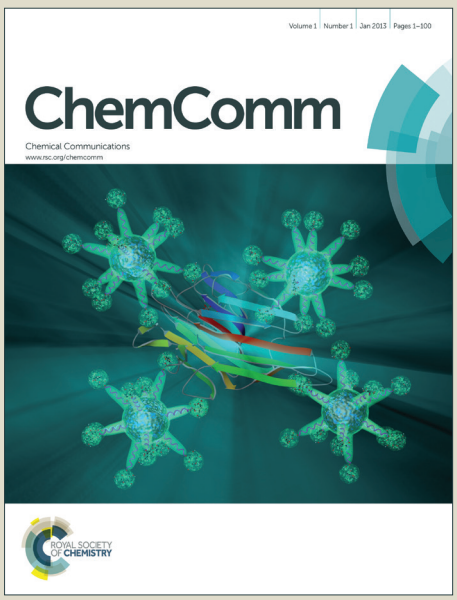

ROYAL SOCIETY OF CHEMISTRY

www.rsc.org/chemcomm

Journal Name

RSCPublishing

COMMUNICATION

Highly efficient bimetal synergetic catalysis of multi-wall carbon nanotubes supported palladium and nickel on hydrogen storage of magnesium hydride†

Cite this: DOI: 10.1039/x0xx00000x

Received 00th January 2012,
Accepted 00th January 2012

DOI: 10.1039/x0xx00000x

www.rsc.org/

Jianguang Yuan [a b], Yunfeng Zhu* [a] and Liquan Li* [a]

Multi-wall carbon nanotubes supported Pd and Ni catalyst efficiently catalyzed hydrogen storage of magnesium hydride prepared by HCS+MM. The excellent hydrogen storage properties were obtained: hydrogen absorption 6.44 wt.% within 100s at 373 K, hydrogen desorption 6.41 wt.% within 1800s at 523 K and 6.70 wt.% within 400s at 573 K.

Hydrogen storage, especially its application in vehicle and hydrogen fuel cell, remains a challenge in the commercialization of an economy based on hydrogen energy.[1] Therefore, the new materials and hydrogen tank systems are needed to meet vehicle requirements. We are trying to produce a new material to store hydrogen on board. Magnesium is a very promising candidate for hydrogen storage material due to its high energy density (43.0 MJ L^{-1}, which meets the DOE hydrogen storage ultimate targets), abundant resources, low cost and non-pollution, attracting extensive research in the last few decades. [2] However, the actual application of magnesium hydride is severely restricted due to its high thermodynamic stability, sluggish hydrogen sorption/desorption kinetics and a severe thermal management.[3] The high thermodynamic stability means that a very high temperature (at least 573 K) is required for desorption. A severe thermal management means that the absorption/desorption of hydrogen requires a heat exchanger with high powers.[4]

To overcome these drawbacks in terms of the materials, several approaches have been adopted to improve the performance of MgH_2 for hydrogen storage, including catalysts addition, alloying, nanostructuring and composite fabrication.[5] Up to now, significant progress has been achieved to enhance the hydrogenation/ dehydrogenation properties. One of the most notable studies is the addition of transition metals as catalysts, such as nickel (Ni), palladium (Pd), cobalt (Co), titanium (Ti), niobium (Nb), copper (Cu), iron (Fe), etc,[6] and some of their compounds have been proven to significantly ameliorate the hydrogen sorption/desorption kinetics of MgH_2. Besides, carbon materials have been widely used as catalyst support in heterogeneous catalysis.[7] Multi-wall carbon nanotubes (MWCNTs), a unique form of carbon, has been demonstrated to be promising alternative support materials owing to their intrinsic properties, such as high surface area, unique electronic properties and chemical inertness, thermal stability and high mechanical strength.[8] Jia et al. synthesized a multi-component catalyst Ni-VO_x on active carbon (AC) and found the Mg-Ni-VO_x/AC composite can absorb 6.2 wt.% hydrogen within only 1 minute at 423 K under a hydrogen pressure of 2 MPa and desorb 6.5 wt% hydrogen within 10 minutes at 573 K.[9]

In the present work, multi-wall carbon nanotubes supported palladium and nickel (Pd_3Ni_3/$MWCNTs_4$, mass ratio) was introduced to the magnesium-based materials by the process of hydriding combustion synthesis (HCS) followed by mechanical milling (MM). Pd_3Ni_3/$MWCNTs_4$ catalyst was synthesized for the first time by a two-step chemical reduction method. The structural properties of the pristine MWCNTs, Ni_3/$MWCNTs_4$ and Pd_3Ni_3/$MWCNTs_4$ catalysts were studied by XRD as shown in Fig. 1. The MWCNTs exhibits a main sharp peak centering at 2θ≈26.4 degree (002). The XRD pattern of the intermediate product Ni_3/$MWCNTs_4$ is shown in Fig. 1(b), which corresponds to the (111), (200) and (220) plane reflections of Ni. The characteristic peaks of Pd corresponding to the

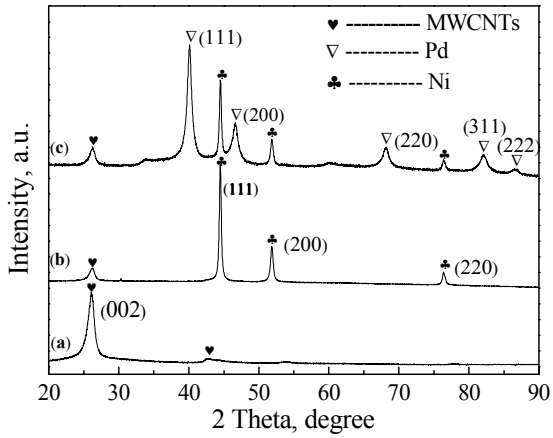

Fig. 1 XRD patterns: (a) MWCNTs, (b) Ni_3/$MWCNTs_4$ catalyst and (c) Pd_3Ni_3/$MWCNTs_4$ catalyst

(111), (200), (220) and (311) plane reflections are observed in Fig. 1(c), confirming the incorporation of Pd and Ni nanoparticles within the Pd_3Ni_3/$MWCNTs_4$ catalyst. The average grain sizes of Pd and Ni are roughly estimated to be about 10.1 and 15.4 nm, respectively.

TEM analysis was used to investigate the dispersion form of the Pd and Ni nanoparticles in the MWCNTs. It can be seen from the

TEM images (Fig. 2 a, b) that the spherical Pd or Ni nanoparticles with a diameter of about 5~20 nm are uniformly distributed on the surface of the MWCNTs. HRTEM micrographs (Fig. 2 c, d) show that the lattice fringes with a separation of 0.1944 nm agree well with the (200) interplanar spacing of Pd; the lattice fringes with a separation of 0.2022 nm agree well with the (111) interplanar spacing of Ni; and the lattice fringes with a separation of 0.3697 or 0.3659 nm agree well with the (002) interplanar spacing of C hexagonal crystal. Furthermore, the inset shows the corresponding selected area electron diffraction (SAED) pattern in Fig. 2(b), which displays a distinguishable ring-like feature and diffraction spots, and the spots from inner to outer correspond to the plane reflections of Ni (200), Pd (311) and C (002). We have performed the EDS mapping of Pd, Ni and C of the as-prepared Pd_3Ni_3/MWCNTs$_4$ as shown in Fig. S1, ESI†. The results clearly indicate that Pd and Ni nano-particles are uniformly distributed on the suface of the MWCNTs.

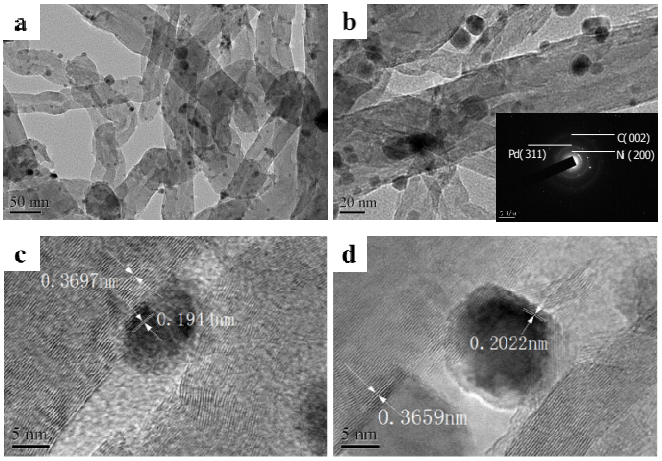

Fig. 2 TEM images of Pd_3Ni_3/MWCNTs$_4$ catalyst: a, b bright field images under different magnifications; c, d HRTEM image; the inset in b gives the corresponding selected area electron diffraction pattern of the Pd_3Ni_3/MWCNTs$_4$ catalyst

Fig. S2(1) shows the XRD patterns of the HCS products of Mg_{95}-(Pd_3Ni_3/MWCNTs$_4$)$_5$, Mg_{95}-(Ni_6/MWCNTs$_4$)$_5$, Mg_{95}-(Pd_6/MWCNTs$_4$)$_5$ and Mg. The peaks of the HCS products mainly correspond to MgH_2 and Mg. No distinct Pd or MWCNTs peaks were detected because of their low abundance. It is noticed that the addition of Pd can significantly increase the hydrogenation degree of Mg during the HCS process and there is hardly un-reacted Mg. The HCS+MM products are shown in Fig. S2(2), which indicates that the diffraction peaks of MgH_2 and Mg are drastically weakened and broadened comparing with that of the HCS products due to grain refinement and lattice stress.

Fig. 3 shows the hydriding curves of the HCS+MM products of Mg, Mg_{95}-(Ni_6/MWCNTs$_4$)$_5$, Mg_{95}-(Pd_6/MWCNTs$_4$)$_5$ and Mg_{95}-(Pd_3Ni_3/MWCNTs$_4$)$_5$ measured at different temperatures of 373 K, 473 K, and 523 K (see Fig. S3, ESI†). As shown in the figure, the HCS+MM product Mg_{95}-(Pd_3Ni_3/MWCNTs$_4$)$_5$ exhibits the best hydriding kinetics at low temperature of 373 K, and even requires only 100 s to reach its saturated hydrogen capacity of 6.44 wt.%. Similarly, Mg_{95}-(Ni_6/MWCNTs$_4$)$_5$ also shows fast hydrogen absorption rate under the same condition, absorbing 5.93 wt.% hydrogen within 100 s. However, for the Mg_{95}-(Pd_6/MWCNTs$_4$)$_5$ and Mg systems, the samples can hardly absorb hydrogen at 373 K, suggesting that Pd has poorer catalytic effect on hydrogen absorption than Ni at 373 K. At 473 K, the rest of the samples show excellent hydriding kinetics except Mg. The hydrogen absorption capacity of Mg_{95}-(Pd_3Ni_3/MWCNTs$_4$)$_5$ is increased to 6.79 wt.%. The hydrogen absorption capacities of all the samples are listed in Table S1, ESI†. Therefore, we can conclude that Ni plays an important role in absorbing hydrogen at low temperature (373 K) and Pd can further increase the hydrogen storage capacity.

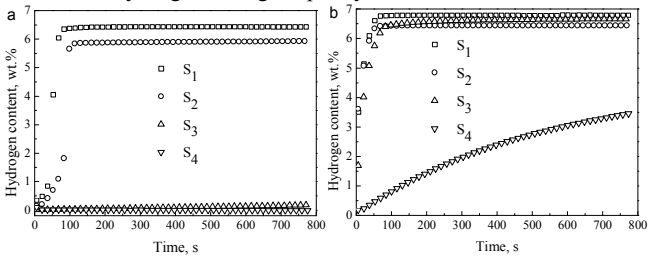

Fig. 3 Hydriding curves of the HCS+MM products: S1 Mg_{95}-(Pd_3Ni_3/MWCNTs$_4$)$_5$, S2 Mg_{95}-(Ni_6/MWCNTs$_4$)$_5$, S3 Mg_{95}-(Pd_6/MWCNTs$_4$)$_5$ and S4 Mg under the initial hydrogen pressure of 3.0 MPa at temperatures of (a) 373 and (b) 473 K, respectively.

The dehydriding curves of the HCS+MM products of Mg, Mg_{95}-(Ni_6/MWCNTs$_4$)$_5$, Mg_{95}-(Pd_6/MWCNTs$_4$)$_5$ and Mg_{95}-(Pd_3Ni_3/MWCNTs$_4$)$_5$ measured at different temperatures of 473 K (see Fig. S4, ESI†), 523 K, and 573 K are shown in Fig. 4. At 523 K, the Mg_{95}-(Pd_3Ni_3/MWCNTs$_4$)$_5$ releases as high as 6.41 wt.% hydrogen within 1800 s, while Mg_{95}-(Ni_6/MWCNTs$_4$)$_5$ releases 3.84 wt.% hydrogen and Mg_{95}-(Pd_6/MWCNTs$_4$)$_5$ releases only 0.52 wt.% hydrogen. Furthermore, at 573 K, the hydrogen desorption capacity of Mg_{95}-(Pd_3Ni_3/MWCNTs$_4$)$_5$ is increased to 6.70 wt.% within only 400 s. The hydrogen desorption capacities of all samples are listed in Table S2, ESI†. This indicates that Pd is more effective for hydrogen desorption.

In order to further study the dehydrogenation properties of the composites, Fig. S5 presents the amount of hydrogen desorbed as a function of temperature of the HCS+MM products. It can be seen that Mg_{95}-(Pd_3Ni_3/MWCNTs$_4$)$_5$ exhibits the fastest dehydriding kinetics, and the dehydriding onset temperature (at which hydrogen begin to release) is about 420 K, which is 60 K lower than that of the Mg. Aminorroaya et al. reported that Mg-10 wt.% Ni alloy co-catalysed with Nb and MWCNTs milled for 60 h shows excellent hydrogen storage properties, absorbing about 5.2 wt.% hydrogen within 100 s at 473 K under a hydrogen pressure of 2.0 MPa, with the dehydriding onset temperature approximately 493 K.[10] The composite in this paper exhibits better hydrogen storage properties.

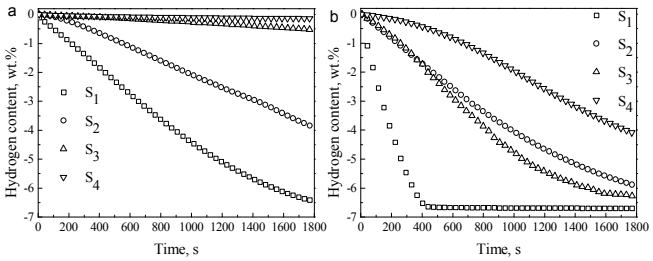

Fig. 4 Dehydriding curves of the HCS+MM products: S1 Mg_{95}-(Pd_3Ni_3/MWCNTs$_4$)$_5$, S2 Mg_{95}-(Ni_6/MWCNTs$_4$)$_5$, S3 Mg_{95}-(Pd_6/MWCNTs$_4$)$_5$ and S4 Mg under 0.005 MPa hydrogen pressure at temperatures of (a) 523 and (b) 573 K, respectively.

Isothermal hydrogenation and dehydrogenation cycling kinetics of the HCS+MM-Mg_{95}-(Pd_3Ni_3/MWCNTs$_4$)$_5$ composite have been measured for 10 cycles at 528 K to prove the cycling stability of the Pd_3Ni_3/MWCNTs$_4$ catalyst. As shown in Fig. S6(a), the de/hydrogenation kinetics of the composite from the 1st to the 10th cycle remains almost the same. The absorbed hydrogen capacity only dwindles from 6.77 wt.% to 6.70 wt.% in Fig. S6(b), which

illustrates the excellent cycling stability of the Mg_{95}-$(Pd_3Ni_3/MWCNTs_4)_5$ system.

The pressure–concentration-isotherms (PCIs) of the HCS+MM-Mg_{95}-$(Pd_3Ni_3/MWCNTs_4)_5$ composite measured at different temperatures of 533 K, 573 K, and 603 K are shown in Fig. S7. Each isotherm has only one hydrogen absorption/desorption plateau corresponding to hydrogenation/dehydrogenation of Mg. The reversible hydrogen capacity of this hydrogen storage system reaches as high as 7.05 wt.% corresponding to 97.2% of the theoretical value of 7.25 wt.%. The corresponding Van't Hoff plot is shown in Fig. S8. The reaction enthalpy of the hydrogenation and dehydrogenation of Mg are calculated as -74.8 and +75.6 kJ mol^{-1} H_2, respectively, which hardly change as compared to the as-received commercial Mg (76 kJ mol^{-1} H_2). Therefore, the thermodynamic property of the composite isn't improved.

To understand the dehydrogenation mechanism, we use the JMA model to describe the desorption mechanism of the composite. The activation energy (E_A) for dehydrogenation is determined by Arrhenius equation after fitting the experimental data. Fig. S9 illustrates the JMA plots of $\ln[-\ln(1-\alpha)]$ vs $\ln(t)$ for the desorption data of HCS+MM-Mg_{95}-$(Pd_3Ni_3/MWCNTs_4)_5$ composite at different temperatures. Fig. S10 shows the Arrhenius plots for the dehydriding kinetics of the composite. The activation energy (E_A) for the dehydrogenation of the composite is calculated as 70.1 kJ mol^{-1} H_2, which is much lower than that of the as-received commercial MgH_2 (153 kJ mol^{-1} H_2).[11]

It is noteworthy that different components in the catalyst function differently in the catalytic effect for the Mg_{95}-$(Pd_3Ni_3/MWCNTs_4)_5$ composite system. Ni nanoparticles help to form intermetallic Mg_2NiH_4 during the HCS process as reaction (1), which is able to store up to 3.6wt% hydrogen, and catalyze efficiently hydrogenation/dehydrogenation of Mg.[12] Fig. S11(1) presents XPS spectra of Ni 2p narrow scan spectra for the HCS+MM-Mg_{95}-$(Pd_3Ni_3/MWCNTs_4)_5$ composite in the dehydrogenated (a) and hydrogenated (b) states. We notice that the binding energies of Ni $2p_{3/2}$ peaks are 852.5 eV (1.37×10^{-16} J) and 850 eV (1.36×10^{-16} J), respectively, corresponding to Mg_2Ni and Mg_2NiH_4.[13] In order to further investigate the catalytic mechanism of Pd, the Pd 3d narrow scan spectra for the HCS+MM composite in the dehydrogenated and hydrogenated states are presented in Fig. S11(2). For the hydrogenated and dehydrogenated samples, the binding energies of Pd $3d_{5/2}$ peaks are 336.9 eV (5.40×10^{-17} J) and 336.1 eV (5.38×10^{-17} J), respectively, corresponding to the alloy MgPd and Mg_6Pd.[14] These values are shifted as compared with the binding energy of pure Pd.[15] Therefore, during the HCS process, the intermetallic MgPd alloy was formed, and we speculate that MgPd might reversibly desorb/absorb hydrogen in three disproportionation reactions as (2)-(4) according to the previous reports: [16]

$$2\,Mg + Ni + 2\,H_2 \Rightarrow Mg_2NiH_4 \quad (1)$$

$$MgPd + 5\,MgH_2 \Leftrightarrow 0.5\,Mg_5Pd_2 + 3.5\,MgH_2 + 1.5\,H_2 \quad (2)$$

$$0.5\,Mg_5Pd_2 + 3.5\,MgH_2 \Leftrightarrow Mg_{3.65}Pd + 2.35\,MgH_2 + 1.15\,H_2 \quad (3)$$

$$Mg_{3.65}Pd + 2.35\,MgH_2 \Leftrightarrow Mg_6Pd + 2.35\,H_2 \quad (4)$$

The nano-sized Mg_2NiH_4, MgPd and some intermediate products release easily hydrogen or react with MgH_2, which makes possible the hydrogen desorption at very low driving forces on the grain boundaries of Mg. Furthermore, because of the two-step preparation method, part of Pd may grow on the Ni surface to form metallic coupling of PdNi. This probably leads to the formation of a new intermetallic compound $Mg_6(Ni,Pd)$ in the composite, which exhibits reversible hydrogen storage at 473 K.[17] It is reasonable to hypothesize that the coupling of PdNi must be more effective on hydrogen absorption and desorption of Mg than Pd or Ni when used individually. Meanwhile, this results in the generation of some new nucleation sites of Mg. MWCNTs also facilitates the atomic hydrogen diffusion from the grain boundaries to the catalysts. Thus, it is quite possible that the dehydrogenation process of MgH_2 becomes easier due to the lower energy needed in the above inferred catalytic process. However, the researching into the reason why the coupling of metals is better than the individuals is very limited and further theoretical investigations are expected.

The microstructure of the milled Mg_{95}-$(Pd_3Ni_3/MWCNTs_4)_5$ was investigated by FESEM. Fig. S12 presents the FESEM image with associated EDS maps for Mg, Ni and Pd. The sample exhibits uniformly-distributed particle size after milling for 10 h, and the average particle size is around 400 nm. The EDS mapping of Mg, Ni and Pd on the same area of the corresponding secondary electron image shows that Ni and Pd exist simultaneously and distribute uniformly, leading to a high catalytic efficiency. The composite in this paper exhibits prominent hydrogen storage properties, which are very favorable to the application of the Mg-based hydrogen storage materials.

This work was supported by the National Natural Science Foundation of China (NSFC) (Grant Nos. 51071085, 51171079), Natural Science Foundation of the Jiangsu Higher Education Institutions of China (Grant No. 13KJA430003), Innovation Foundation for Graduate Students of Jiangsu Province (Grant No. CXZZ12_0408, CXZZ13_0420), Qing Lan Project and the Priority Academic Program Development (PAPD) of Jiangsu Higher Education Institutions.

Notes and references

[a] *College of Materials Science and Engineering, Nanjing Tech University, 5 Xinmofan Road, Nanjing, 210009, P.R. China.*
E-mail: yfzhu@njtech.edu.cn; lilq@njtech.edu.cn; Tel: +86-25-83587255
[b] *Doctor student*

† Electronic Supplementary Information (ESI) available: [Experimental, Characterization of samples, Table S1, S2, Fig. S1~S12]. See DOI: 10.1039/c000000x/

1 (a) U. Eberle, B. Müller and R. V. Helmolt, *Energy Environ. Sci*., 2012, **5**, 8780 – 8798; (b) L. Schlapbach and A. Züttel, *Nature*, 2001, **414**, 353-354; (c) G. Marbán and T. Valdés-Solís, *Int. J Hydrogen Energy*, 2007, **32**, 1626.

2 (a) J. Yang, A. Sudik, C. Wolverton and D. J. Siegel, *Chem. Soc. Rev*., 2010, **39**, 656-675; (b) D. K. Ross, *Vacuum*, 2006, **80**, 1084-1089; (c) M. Felderhoff, C. Weidenthaler, R. V. Helmolt and U. Eberle, *Phys. Chem. Chem. Phys.*, 2007, **9**, 2643-2653.

3 (a) B. Sakintuna, F. Lamari-Darkrim and M. Hirscher, *Int. J Hydrogen Energy*, 2007, **32**, 1121-1140; (b) J. Yang, A. Sudik, C. Wolverton and D.J. Siegel, *Chem. Soc. Rev.*, 2010, **39**, 656-657; (c) K-F. Aguey-Zinsou and J-R. Ares-Fernández, *Energy Environ. Sci.*, 2010, **3**, 526-543.

4 (a) D. Mori and K. Hirose, *Int. J Hydrogen Energy*, 2009, **34**, 4568-4574; (b) R. Bardhan, A. M. Ruminski, A. Brand and J. J. Urban, *Energy Environ. Sci*., 2011, **4**, 4882-4895. (c) F. Y. Cheng, Z. L. Tao, J. Liang and J. Chen, *Chem. Commun.*, 2012, **48**, 7334-7343; (d) A. F. Dalebrook, W. J. Gan, M. Grasemann, S. Moretand and G. Laurenczy, *Chem. Commun*., 2013,**49**, 8735-8751.

5 (a) M. X. Gao, J. Gu, H. G. Pan, Y. L. Wang, Y. F. Liu, C. Liang and Z. X. Guo, *J. Mater. Chem*., 2013, **1**, 12285-12292; (b) O. Gutfleisch, S. Dal Toè, M. Herrich, A. Handstein and A. Pratt, *J Alloys Compd*., 2005, **404-406**, 413-416; (c) C. Y. Zhu, S. Hosokai and T. Akiyama, *Cryst. Growth. Des*., 2011, **11**, 4166-4174; (e) K-J. Jeon, H. R. Moon,

A. M. Ruminski, B. Jiang, C. Kisielowski and R. Bardhan, *Nat. Mater*., 2011, **10**, 286-290.

6 (a) G. X. Tan, C. T. Harrower, B. S. Amirkhiz and D. Mitlin, *Int. J Hydrogen Energy*, 2009, **34**, 7741-7748; (b) E. Callini, L. Pasquini, L. H. Rude, T. K. Nielsen, T. R. Jensen and E. Bonetti, *J Appl. Phys*., 2010, **108**, 073513-073517; (c) Y. Wu, M. V. Lototsky, J. K. Solberg, V. A. Yartys, W. Han and S. X. Zhou, *J Alloys Compd*., 2009, **477**, 262-266; (e) H. Gu, Y. F. Zhu and L. Q. Li, *Int. J Hydrogen Energy*, 2009, **34**, 2654-2660.

7 (a) Y. Jia, J. Zou and X. D. Yao, *Int. J Hydrogen Energy,* 2012, **37**, 13393-13399; (b) X. C. Dong, Y. Ma, G. Zhu, Y. Huang, J. Wang, M. B. Chan-Park, L. Wang, W. Huang and P. Chen, *J. Mater. Chem*., 2012, **22**, 17044; (c) S. Aminorroaya, A. Ranjbar, Y-H. Cho, H. K. Liu and A. K. Dahle, *Int. J Hydrogen Energy*, 2011, **36**, 571-579.

8 (a) G. G. Wildgoose, C. E. Banks and R. G. Compton, *Small*, 2006, **2**, 182; (b) M. L. Brandl, J. M. P. van Heeswijk, J. H. Bitter, A. J. van Dillen and K. P. de Jong, *Carbon*, 2004, **42**, 307.

9 Y. Jia, L. Cheng, N. Pan, J. Zou, G. Q. Lu and X. D. Yao, *Adv. Energy Mater*., 2011**, 1**, 387-393.

10 S. Aminorroaya, A. Ranjbar, Y. H. Cho, H. K. Liu and A. K. Dahle, *Int. J Hydrogen Energy*, 2011, **36**, 571-579.

11 Y. J. Choi, J. Lu, H. Y. Sohn and Z. Z. Fang, *J. Power Sources*, 2008, **180**, 491-497.

12 (a) L. Q. Li, T. Akiyama and J-i. Yagi, *Int J. Hydrogen Energy*, 2001, **26**, 1035-1040; (b) H. Gu, Y. F. Zhu and L. Q. Li, *Mater. Chem. Phys*., 2008, **112**, 218-222.

13 (a) A. Montone, J. G. Novakovic, M. V. Antisari, A. Bassetti, E. Bonetti, A. L. Fiorini, L. Pasquini, L. Mirenghi and P. Rotolo, *Int. J Hydrogen Energy*, 2007, **32**, 2926-2934; (b) P. Selvam, B. Viswanathan and V. Srinivasan, *Int. J Hydrogen Energy*, 1989, **14**, 899-902.

14 L. Pasquini, F. Boscherini, E. Callini, C. Maurizio, L. Pasquali, M. Montecchi, and E. Bonetti, *Phys. Rev. B*., 2011, **83**, 184111.

15 C. Zlotea and Y. Andersson, *Acta Mater*., 2006, **54**, 5559-5564.

16 (a) J. P. A. Makongo, Y. Prots, U. Burkhardt, R. Niewa, C. Kudla and G. Kreiner, *Taylor & Francis*, 2006, **86**, 427-433; (b) J. Dufour and J. Huot, *J Alloys Compd*., 2007, **446-447**, 147-151.

17 J. F. Fernandez, J.R. Ares, F. Cuevas, J. Bodega, F. Leardini and C. Sa´nchez, *Int J. Hydrogen Energy*, 2001, **36**, 14496-14502

